Study on modeling of flow induced noise using Lighthill's analogy and boundary element method

Masaaki MORI[1]; Takayuki MASUMOTO[2]; Kunihiko ISHIHARA[3]; Takuya OSHIMA[4]; Yosuke YASUDA[5]; Tetsuya SAKUMA [6]

[1] CYBERNET SYSTEMS CO., LTD, Japan

[2] CYBERNET SYSTEMS CO., LTD, Japan

[3] Tokushima Bunri University, Japan

[4] Niigata University, Japan

[5] Kanagawa University, Japan

[6]The University of Tokyo, Japan

ABSTRACT

We have calculated the flow-induced sound pressure field using Lighthill's acoustic analogy by means of an acoustic boundary element method (BEM). For this calculation, firstly, an unsteady flow field is calculated using a computational fluid dynamics (CFD) solver. Then acoustic sources are extracted from the result and transformed into the frequency domain. Finally, these are used as quadrupole acoustic sources in the acoustic BEM model. In the BEM calculation, because some of the CFD grid points exist quite close to the BEM elements, for example 100 times smaller than the element length, so the contribution from the sources must be evaluated quite preciously. To achieve this, the elemental integration of the source contribution is introduced. We have validated the procedure (CFD/BEM approach) by comparing with an experimental data. The first validation is a comparison of the acoustic pressure generated by a low Mach number flow past a 3D circular cylinder. The second validation is a comparison of the acoustic pressure induced by a low Mach number flow in a bending duct. Finally the transmitting acoustic pressure which is originally induced by a flow through an elastic structure is calculated by the structural-acoustic coupled model.

Keywords: Flow-induced sound, Lighthill's acoustic analogy, BEM, Structural-acoustic coupling, I-INCE Classification of Subjects Number(s): 21.6

1. INTRODUCTION

An acoustic analogy has been widely used to compute aeroacoustics (1). In this method, an unsteady flow field must be calculated to obtain the acoustic source information, and the propagation of the far-field acoustic pressure are predicted mainly using Curle's equation (2), Ffowcs Williams-Hawkings equation (3) or finite element method (FEM) based on Lighthill's analogy (4,5) .

FEM is widely used to compute the acoustic field in industry. This is due to its benefit such as possibility of modeling sound speed distribution in the field, eventually it leads to the capability of an acoustic analysis with the existence of a mean flow. However, because it requires the field to be discretized with volume elements, as the size of the field become large or the frequency become high, the huge calculation cost is required. On the other hand, boundary element method (BEM) has also been widely used especially for analyzing the external acoustic field excited by for example the structural vibration. Because it only requires the boundary of the field to be discretized with surface elements, the number of DOF is

[1]m-mori@cybernet.co.jp
[2] masumoto@cybernet.co.jp
[3] k-ishihara@fe.bunri-u.ac.jp
[4] oshima@eng.niigata-u.ac.jp
[5] yyasuda@kanagawa-u.ac.jp
[6] sakuma@k.u-tokyo.ac.jp

drastically smaller than FEM, and the radiated acoustic field can be modeled smartly (the Sommerfeld radiation condition is fulfilled automatically).

In this study, the flow-induced far-field acoustic characteristics are calculated based on Lighthill's analogy by means of BEM. In this procedure acoustic sources are extracted from CFD results (CFD/BEM approach). As for CFD, three types of model are used such as a low Mach number flow past a 3D circular cylinder, a low Mach number flow in a bending duct and a low Mach number flow in a T-shaped rectangular cross-sectional pipe. The results are validated by comparing with the experimental data.

2. Numerical Procedure

2.1 Transient CFD simulation

2.1.1 Low Mach number flow past the 3D circular cylinder

The turbulence vortex shedding from a 3D circular cylinder of diameter D = 10 mm and span L = 20D is simulated at Re = 26,000 and M = 0.11765 (U = 40 m/s). The model used for the CFD simulation is shown in Figure 1. For this Simulation, a three-dimensional rectangular computational domain around the cylinder has been applied. The unsteady flow field is calculated using the CFD code ANSYS CFX (6) version 15.0 and its incompressible LES (Dynamic Smagorinsky model) calculation features. There are 1,550,000 cells and 1,588,730 nodes in the computational domain (14D×10D×20D). The origin of the Cartesian coordinate is placed at the midpoint of the 3D circular cylinder. A steady velocity is imposed on the inflow boundary. No-slip conditions are applied on the cylinder and side walls. Slip-conditions are applied on the top and bottom boundaries. On the other boundary, a zero pressure outflow condition is applied. A steady state simulation was performed and used as the initial condition of the transient simulation. The transient simulation was performed for 11,500 time steps with the time step size Δt = 5e-5 s.

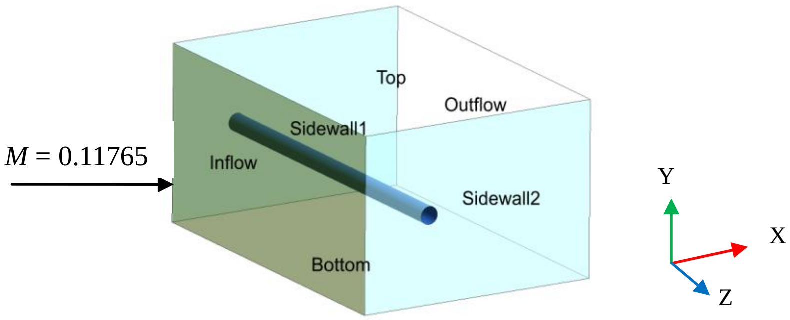

Figure 1 – Domain shape of the 3D cylinder case

2.1.2 Low Mach number flow in the bending duct

The low Mach number flow in the bending square duct of diameter D = 200 mm is simulated at Re = 253,297 and M = 0.0544 (U = 18.5 m/s). The model used for the CFD simulation is shown in Figure 2. For this Simulation, a three-dimensional computational domain in the bending square duct has been applied. The unsteady flow field is calculated using the CFD code ANSYS Fluent (7) version 15.0 and its incompressible LES (Dynamic Smagorinsky model) calculation features. There are 804,300 cells and 831,362 nodes in the computational domain. A steady velocity is imposed on the inflow boundary. A zero pressure outflow condition is applied on the outflow boundary. No-slip conditions are applied on the other walls. A steady state simulation was performed and used as the initial condition of the transient simulation. The transient simulation was performed for 9,000 time steps with the time step size Δt = 1e-4 s.

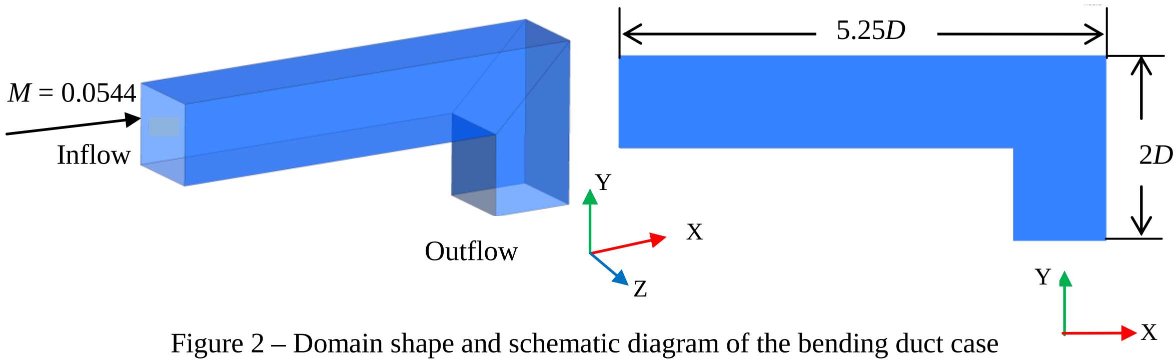

Figure 2 – Domain shape and schematic diagram of the bending duct case

2.1.3 Low Mach number flow in the T-shaped rectangular cross-sectional pipe

The low Mach number flow in the T-shaped rectangular cross-sectional pipe of diameter D = 100 mm is simulated at Re = 90,606 and M = 0.0177 and 0.0412 (U = 6 and 14 m/s). The model used for the CFD simulation is shown in Figure 3. For this Simulation, a three-dimensional computational domain in the T-shaped rectangular cross-sectional pipe has been applied. The unsteady flow field is calculated using the CFD code ANSYS CFX (6) version 15.0 and its incompressible LES (Dynamic Smagorinsky model) calculation features. The origin of the Cartesian coordinate is placed at the midpoint of the T-shaped rectangular cross-sectional pipe case. A steady velocity is imposed on the inflow boundary. Zero pressure outflow conditions are applied on the outflow boundaries. No-slip conditions are applied on the other walls. A steady state simulation was performed and used as the initial condition of the transient simulation. The transient simulation was performed for 2,500 time steps with the time step size Δt = 1e-4 s.

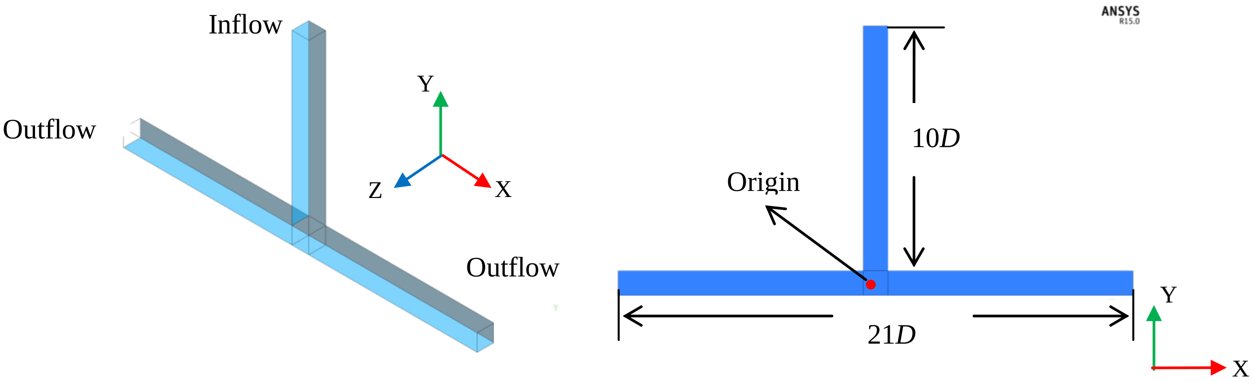

Figure 3 – Domain shape and schematic diagram of the T-shaped rectangular cross-sectional pipe case

2.2 Lighthill Equation

The Lighthill equation in the frequency domain (1) is derived from the equation of continuity and compressible Navier-Stokes equation and as follows.

$$(\nabla^2 + k^2)p = \frac{\partial T_{lm}}{\partial x_l \, \partial x_m} \tag{1}$$

$$T_{lm} = \rho v_l v_m + (p - c^2 \rho)\delta_{lm} \tag{2}$$

where p is the acoustic pressure, k is the wave number, ρ is the density, c is the speed of sound, l and m indicate each direction in the Cartesian coordinates, v is the flow velocity and T_{lm} are coefficients of the Lighthill stress tensor.

2.3 Extraction of Acoustic Source Data

To convert the acoustic time histories into the frequency spectra, a discrete Fourier transform (DFT) has been applied. A frequency increment Δf and a sampling period are 10 Hz and 5e-5 s respectively for the 3D cylinder case, about 1.6 Hz and 6e-4 s for the bending duct case and 5 Hz and 2e-4 s for the T-shaped rectangular cross-sectional pipe case.

2.4 Boundary Element Model

The BEM solver in CYBERNET SYSTEM's acoustic simulation package, WAON (8), is used to solve the acoustic characteristics. In this solver, the following simultaneous linear equation is solved.

$$(\boldsymbol{E}+\boldsymbol{B}+\boldsymbol{C})\boldsymbol{p}=j\omega\rho\boldsymbol{A}\boldsymbol{v}+\boldsymbol{p}_{\mathrm{d}} \tag{3}$$

where $\boldsymbol{p}$ is the acoustic pressure vector, $\boldsymbol{v}$ is the particle velocity vector and the entries of the influence coefficient matrices are represented respectively, by $E_{ij}=\frac{1}{2}\delta_{ij}$, $A_{ij}=\int_{\Gamma_1} N_j(\boldsymbol{r}_q)G(\boldsymbol{r}_i,\boldsymbol{r}_q)dS_q$, $B_{ij}=\int_{\Gamma} N_j(\boldsymbol{r}_q)\frac{\partial G(r_i,r_q)}{\partial n_q}dS_q$, $C_{ij}=\frac{jk}{Z_j}\int_{\Gamma_2} N_j(\boldsymbol{r}_q)G(\boldsymbol{r}_i,\boldsymbol{r}_q)dS_q$, δ_{ij} is Kronecker's delta, Γ_1 is a part of the total boundary Γ where the surface is assumed to be vibrating, Γ_2 is also a part of Γ where the surface absorbs acoustic wave, $\boldsymbol{r}_i$ is the position vector of the i-th node, and N_j is the interpolation function of the j-th node, to give $p(\boldsymbol{r}_q)=\sum_{j=1}^{N} N_j(\boldsymbol{r}_q)p_j$ with the number of nodes N. The vector $\boldsymbol{p}_{\mathrm{d}}$ is the direct pressure contribution from the acoustic source which is evaluated by the following equation.

$$p_{\mathrm{d}}(\mathbf{r}_{\mathrm{p}})=\frac{-1}{4\pi}\sum_l\sum_m\frac{\partial^2}{\partial x_l\partial x_m}\int\frac{T_{lm}(\boldsymbol{r}_s,\omega)\mathrm{e}^{jk|r_p-r_s|}}{|\boldsymbol{r}_p-\boldsymbol{r}_s|}d\mathrm{V} \tag{4}$$

where $\partial^2/\partial x_l\partial x_m$ is the directional derivative and V is the volume of the flow field (in this case, the region filled by CFD cell) respectively.

There are 1,200 boundary elements for the 3D cylinder case, 2,780 elements for the bending duct case and 21,620 for the T-shaped rectangular cross-sectional pipe case, respectively. Acoustic sources are extracted from CFD results whose numbers are equivalent to the number of grids of the CFD model. Figure 4, 5 and 6 show boundary elements in each case. Absorption boundary conditions are imposed at inflow boundaries for both the bending duct case and the T-shaped rectangular cross-sectional pipe case. In the T-shaped rectangular cross-sectional pipe case, in order to avoid the direct contribution from acoustic sources, additional rectangular tubes are modeled at outsides of outflow surfaces and absorption boundary conditions are imposed at all additional surfaces. All other surfaces are assumed to be rigid.

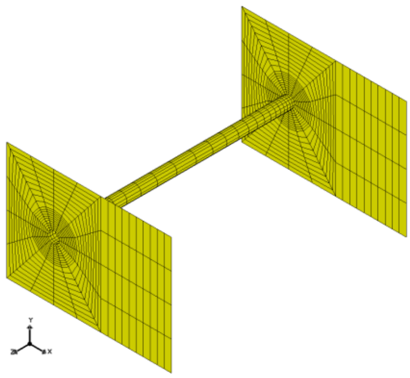

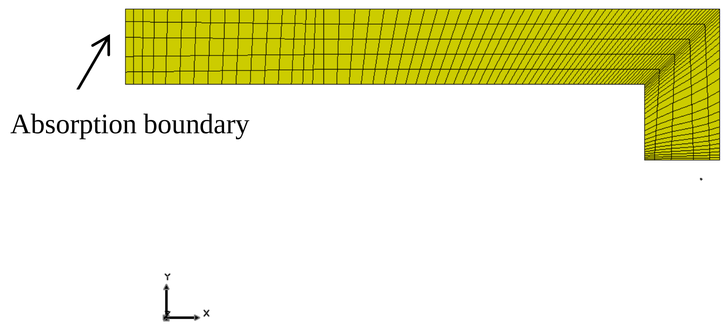

Figure 4 – Boundary element mesh for the 3D cylinder case (Left)
Figure 5 – Boundary element mesh for the bending duct case (Right)

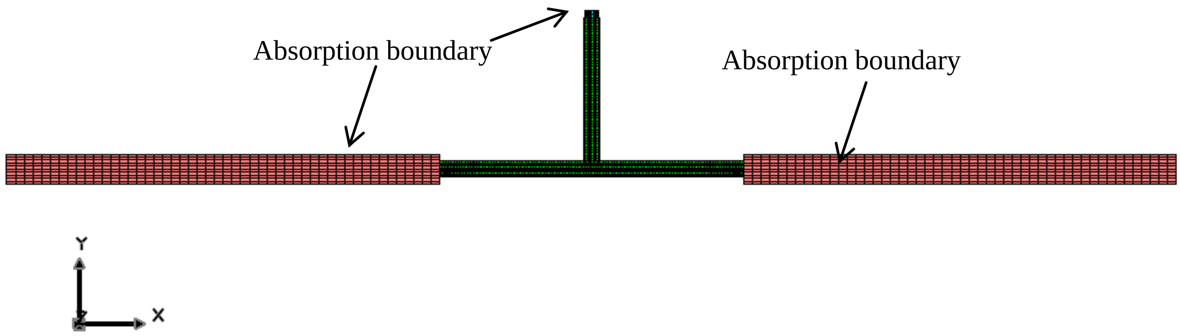

Figure 6 – Boundary element mesh for the T-shaped rectangular cross-sectional pipe case

2.5 Structural-Acoustics Coupling

In this paper, the structural-acoustic coupled model is solved for the T-shaped rectangular cross-sectional pipe case. In order to solve structural-acoustic coupled model, equations corresponding to the acoustic field and the structure must be solved simultaneously.

Displacement of the structure is described, using equation of motion, as

$$(-\omega^2\boldsymbol{M}-\omega\boldsymbol{C}+\boldsymbol{K})\boldsymbol{u}=\boldsymbol{f}_s \tag{5}$$

where $\boldsymbol{M}$: Mass matrix, $\boldsymbol{C}$: Damping matrix, $\boldsymbol{K}$: Stiffness matrix, $\boldsymbol{f}_s$: Excitation force vector.

With modal coordinates, we obtain,

$$(-\omega^2-2jh\omega\boldsymbol{\omega}_0+\boldsymbol{\omega}_0^2)\boldsymbol{q}=\boldsymbol{\varphi}^{\mathrm{T}}\boldsymbol{f}_s \tag{6}$$

where h: Modal damping ratio, $\boldsymbol{\omega}_0$: A matrix in which eigenvalues are arranged diagonally, $\boldsymbol{\varphi}^{\mathrm{T}}$: Eigenvector transposition, $\boldsymbol{q}$: Modal participation factor.

In order to consider the acoustic contribution to the structural model, an additional force term from the acoustic field is introduced.

$$(-\omega^2-2jh\omega\boldsymbol{\omega}_0+\boldsymbol{\omega}_0^2)\boldsymbol{q}=\boldsymbol{\varphi}^{\mathrm{T}}(\boldsymbol{f}_s-\boldsymbol{p}s) \tag{7}$$

where s is the area affected by the acoustic pressure.

On the other hand, to consider the structural contribution to the acoustic model, an additional velocity term from the structure is introduced to eq. (3).

$$(\boldsymbol{E}+\boldsymbol{B}+\boldsymbol{C})\boldsymbol{p}=j\omega\rho\boldsymbol{A}\boldsymbol{v}+j\omega\rho\boldsymbol{A}'\boldsymbol{v}_s \tag{8}$$

where $\boldsymbol{v}_s$: Vibration velocity vector of the structural model and

$$A'_{ij}=\int_{\Gamma_3}N_j(\boldsymbol{r}_q)G(\boldsymbol{r}_i,\boldsymbol{r}_q)dS_q \tag{9}$$

where Γ_3 is the boundary on which structural-acoustic coupled effect is considered.

The term $\boldsymbol{v}_s$ in eq. (8) is modified into an expression in which modal coordinates are used; this is then combined with eq. (7) to obtain the following coupled equation of acoustic and structural models.

$$\begin{bmatrix}\boldsymbol{E}+\boldsymbol{B}+\boldsymbol{C} & \omega^2\rho\boldsymbol{A}'\boldsymbol{\varphi}\\ -\boldsymbol{\varphi}^{\mathrm{T}}s & -\omega^2-2jh\omega\boldsymbol{\omega}_0+\boldsymbol{\omega}_0^2\end{bmatrix}\begin{Bmatrix}\boldsymbol{p}\\ \boldsymbol{q}\end{Bmatrix}=\begin{Bmatrix}j\omega\rho\boldsymbol{A}\boldsymbol{v}\\ \boldsymbol{\varphi}^{\mathrm{T}}\boldsymbol{f}_s\end{Bmatrix} \tag{10}$$

A modal analysis has been performed in the T-shaped rectangular cross-sectional pipe case using ANSYS Mechanical (9) version 15.0. Figure 8 shows boundary conditions in the modal analysis.

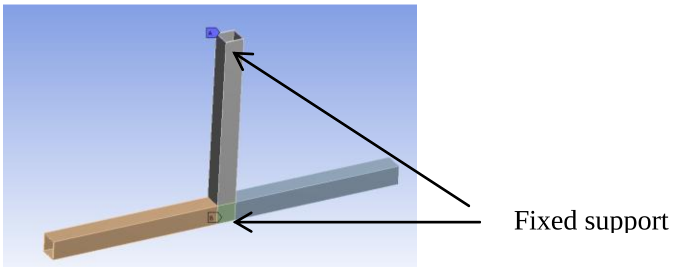

Figure 8 – Boundary conditions in the modal analysis

Young's Modulus, Poisson's ratio and density of the T-rectangular pipe are respectively, 3.14 GPa, 0.35 and 1190 kg/m^3. Figure 9 shows typical shape modes as results of modal analysis.

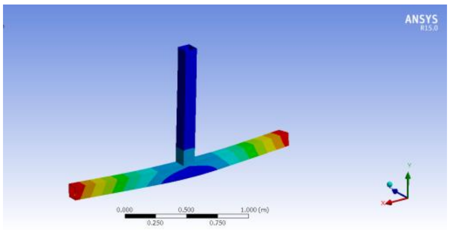

3rd mode at f = 34.061 Hz

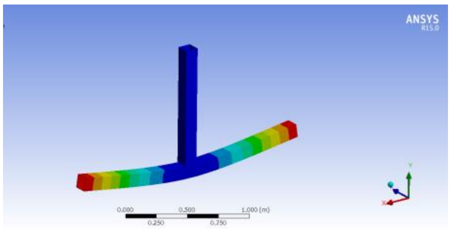

4th mode at f = 34.168 Hz

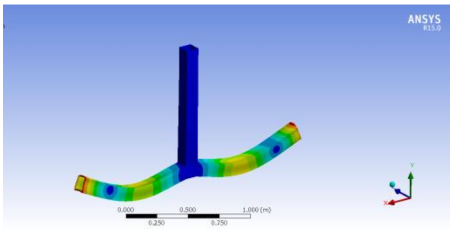

10th mode at f = 190.31 Hz

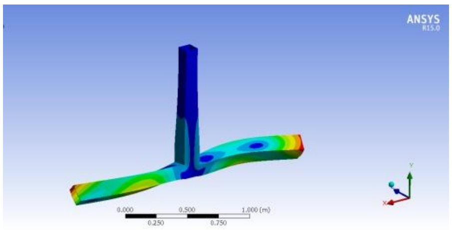

11th mode at f = 190.35 Hz

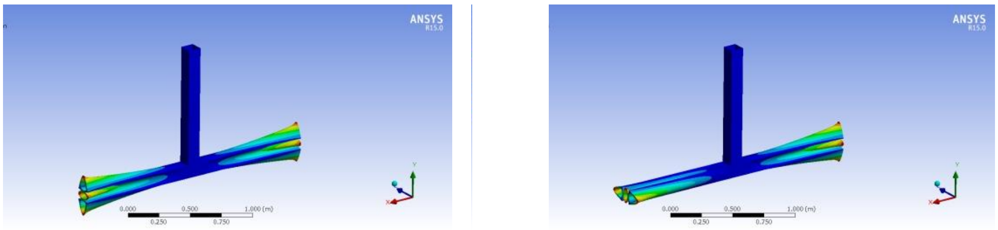

21st mode at f = 353.76 Hz 22nd mode at f = 353.76 Hz

Figure 9 – Typical shape modes of modal analysis

3. Results and Discussions

3.1 Low Mach number flow past the 3D circular cylinder

3.1.1 Transient CFD Results

Figure 10 shows an instantaneous snapshot of an isocontour of the Q criterion factor in the flow field. The Q criterion (vortices) generated at the cylinder surface is shed from the cylinder and travels downstream.

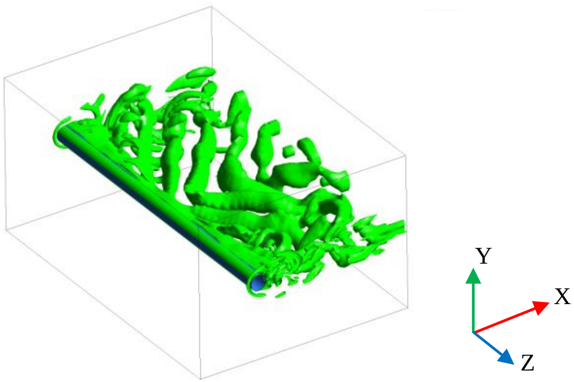

Figure 10 – Instantaneous snapshot of an isocontour of the Q criterion factor (Q = 500000)

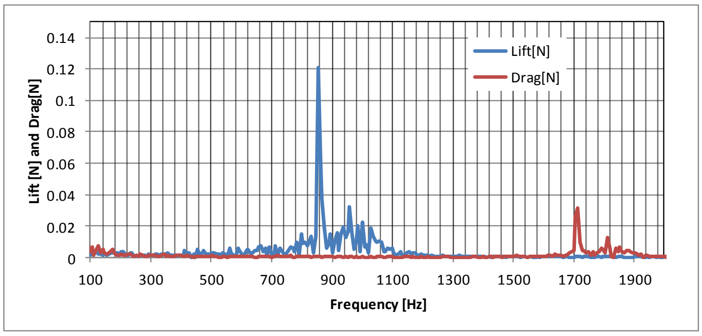

Figure 11 – Frequency spectra of lift and drag forces

Figure 11 shows the frequency spectra of the fluctuating lift and drag forces exerted on the cylinder. The fundamental vortex shedding frequency is about 859 Hz. The mean drag coefficient and the Strouhal number calculated from the transient CFD simulation are respectively, Cd = 1.069, St = 0.214, and they are in good agreement with experimental values reported by Zdravkovich (10) and Ishihara (12). Figure 12 shows instantaneous snapshots of Lighthill Stress tensor $\rho u_l u_m$ at Z = 0 plane. Significant acoustic sources exist near the cylinder and in the wake of the cylinder.

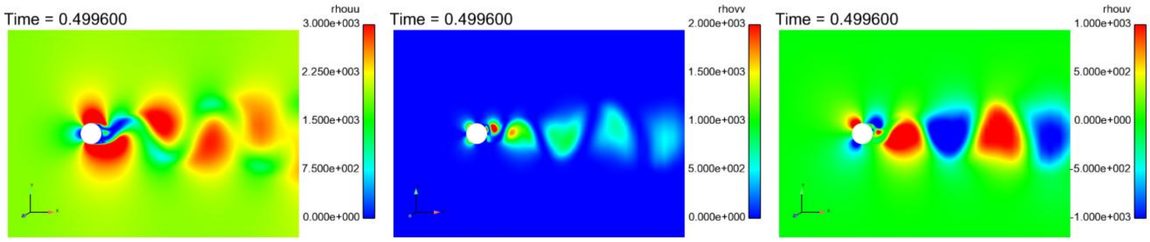

$\rho u_1 u_1$ $\rho u_2 u_2$ $\rho u_1 u_2$

Figure 12 – Instantaneous snapshots of the Lighthill Stress tensor $\rho u_l u_m$ at t = 0.4996s and Z = 0 plane.

3.1.2 **Far-Field Acoustics**

Contours of the sound pressure level at both the fundamental vortex shedding frequency, 859 Hz and its high harmonic frequency, 1710 Hz, are given in Figure 13. Figure 13(a) shows a dipolar nature of the acoustic pressure and the lift dipole dominates the acoustic pressure field at 859 Hz. Also, the drag dipole dominates the acoustic pressure field at 1710 Hz in Figure 13(b). It is assumed that the acoustic pressure radiated by acoustic quadrupole sources are scattered due to the existence of the solid wall, and as a result, the acoustic pressure field has the dipolar nature (11). Figure 14 shows a comparison between the measured and simulated spectral sound pressures level (SPL) at (0, 50*D*, 0). As shown in Figure 14, the acoustic pressure obtained by the simulation satisfactorily agrees with the result of the experiment (12).

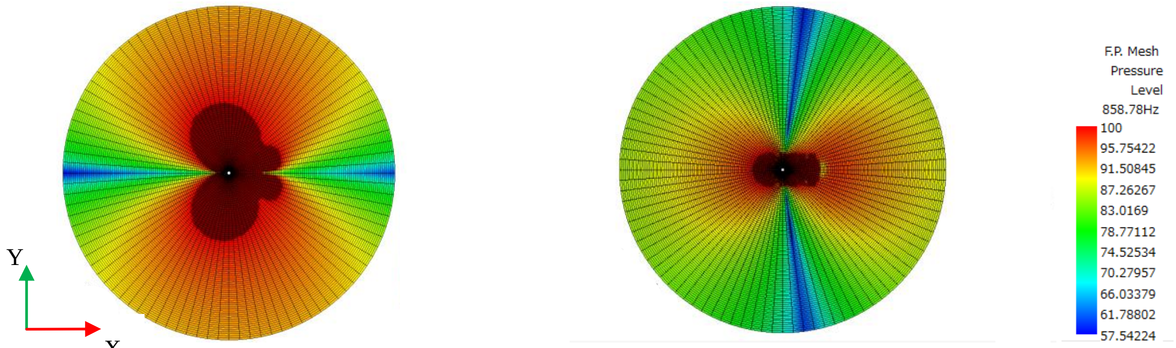

(a) 859 Hz (b) 1710 Hz

Figure 13 – Sound pressure level at Z = 0 plane

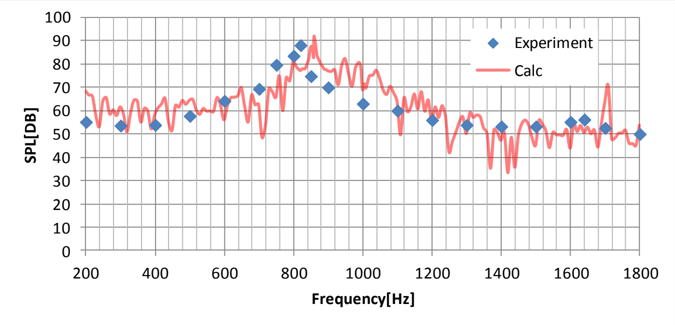

Figure 14 –Spectra of sound pressure levels at (0, 50D, 0)

3.2 **Low Mach number flow in the bending duct**

3.2.1 **Transient CFD Results**

Figure 15 shows an instantaneous snapshot of the vorticity field in the flow field at Z = 0 plane. Vortices generated near corners of the duct are shed from the corner and travels downstream.

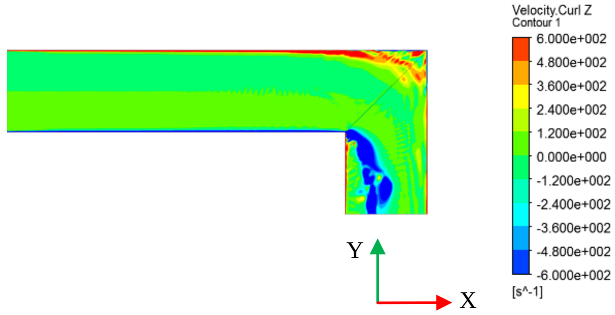

Figure 15 – Instantaneous snapshot of contour of vorticity field

Figure 16 shows instantaneous snapshots of Lighthill Stress tensor $\rho u_l u_m$ at Z = 0 plane. It shows that significant acoustic sources exist near corners of the duct.

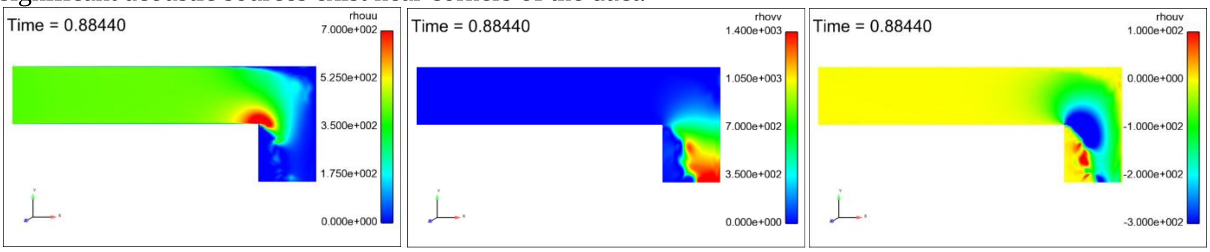

$\rho u_1 u_1$ $\rho u_2 u_2$ $\rho u_1 u_2$

Figure 16 – Instantaneous snapshots of the Lighthill Stress tensor $\rho u_l u_m$ at t = 0.8844s and Z = 0 plane.

3.2.2 Far-Field Acoustics

Figure 17 shows a comparison between the measured and simulated spectral SPL at a position, which is located at 100 mm and 45° from the center of the outflow boundary. It shows that the acoustic pressure obtained by the simulation satisfactorily agrees with the experimental result (13).

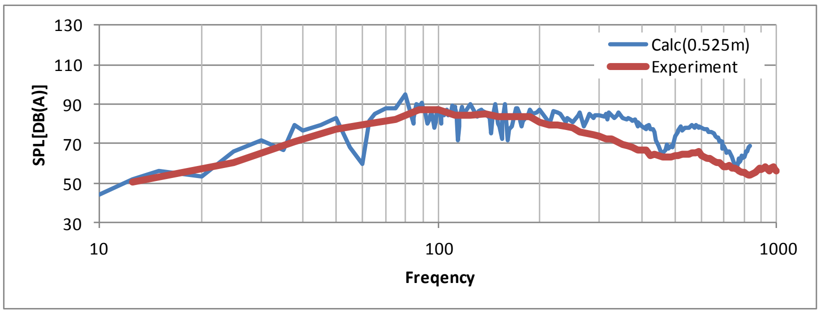

Figure 17 –Spectra of sound pressure levels

3.3 Low Mach number flow in the T-rectangular pipe

3.3.1 Transient CFD Results

Figure 18 shows an instantaneous snapshot of the vorticity field at Z = 0 plane in the case of U = 14 m/s. Vortices generated near corners of the T-shaped rectangular cross-sectional pipe are shed from the corner and travels downstream. Shed vortices merges and interacts with the pipe wall. Motions of these vortices play an important role of the sound generation. Figure 19 shows instantaneous snapshots of Lighthill Stress tensor $\rho u_l u_m$ at Z = 0 plane in the case of U = 14 m/s. It shows that significant acoustic sources exist near corners and the wall of the pipe, as in the vorticity field.

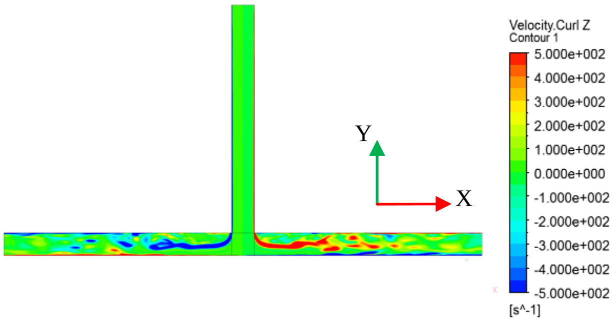

Figure 18 – Instantaneous snapshot of contour of vorticity field (U = 14 m/s).

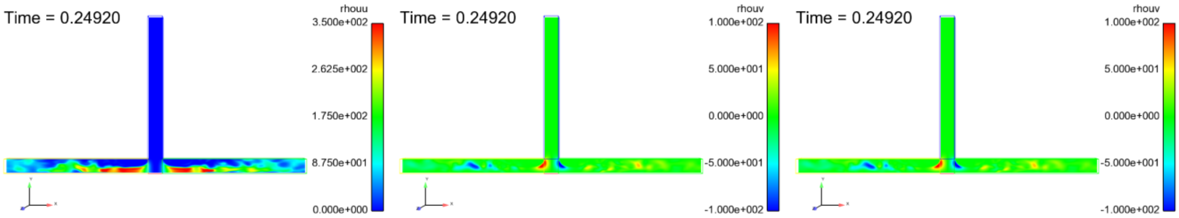

$\rho u_1 u_1$ $\rho u_2 u_2$ $\rho u_1 u_2$

Figure 19 – Instantaneous snapshots of the Lighthill Stress tensor $\rho u_l u_m$ at t = 0.25s and Z = 0 plane (U = 14 m/s).

3.3.2 Far-Field Acoustics

To investigate the effect of the structural-acoustic coupling, we have calculated both the coupled and uncoupled acoustic pressure field. Figure 20 shows the frequency spectra of SPL at a position, which is located at 10mm from the center of the outflow boundary. It shows the difference of frequency spectra peaks between the coupled and uncoupled acoustic pressure. It indicates that the frequency characteristics of the acoustic pressure generated in the pipe changes due to the vibration of the elastic structure. Figure 21 shows the frequency spectra of the transmitted acoustic pressure to the outside of the pipe, which is located at (5.6D, 0.8D, 0). It shows that the first peak frequency is about 34.18 Hz, and corresponds to 3rd and 4th frequencies of modal analysis in Figure 9. Also, other peak frequencies correspond to modal frequencies in Figure 9. Figure 22 shows contours of the SPL at 34.18 Hz and 190.43 Hz in the case of U = 14 m/s. The frequency characteristics of the transmitted acoustic pressure are different from that of the acoustic pressure generated in the pipe. It means that to evaluate the transmission of the acoustic pressure generated by the flow in the pipe, the effect of the structural-acoustic coupling should be taken into consideration. A comparison between the calculated data and an experimental data will be performed in the near future.

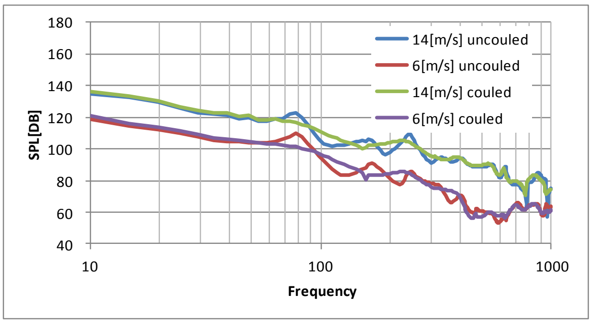

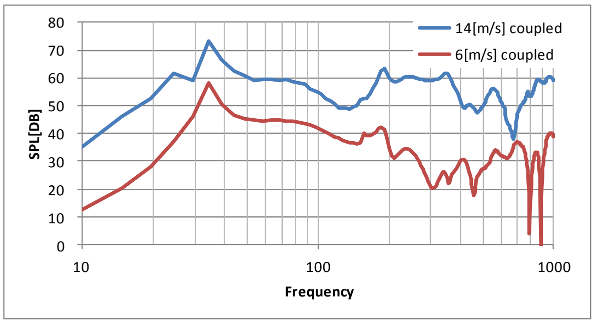

Figure 20 –Spectrum of sound pressure levels near the outflow boundary (Left)
Figure 21 –Spectrum of sound pressure levels in the outside of the pipe (Right)

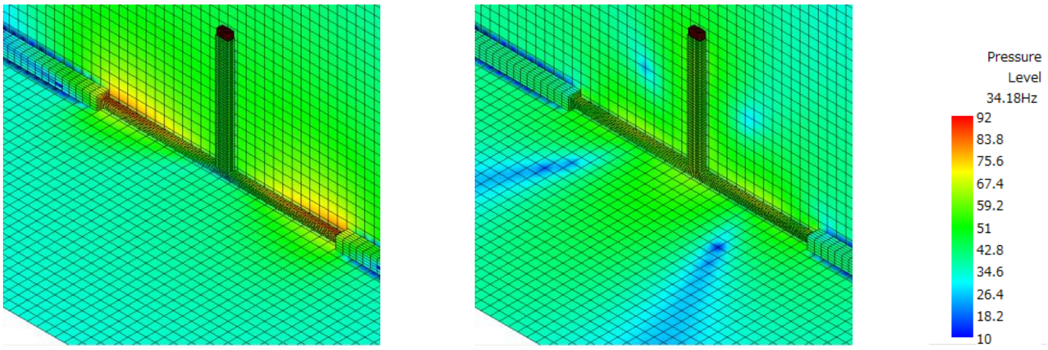

Figure 22 –Sound pressure level at 34.18 Hz and 190.43 Hz in the case of U = 14 m/s.

4. CONCLUSIONS

The flow-induced sound pressure using the Lighthill's acoustic analogy by means of BEM has been simulated and validated by comparing with the experimental data. In the case of the flow past the 3D circular cylinder, the simulated acoustic pressure field shows the lift dipolar nature and satisfactorily agrees with the experimental data. Also, in the case of the flow in the bending duct, the simulated data satisfactorily agrees with the experimental data. In the case of the flow in the T-rectangular pipe, the effect of the structural-acoustic coupling has been studied. The frequency characteristics of the acoustic pressure generated in the pipe is affected by the vibration of the elastic structure. Peak frequencies of the transmitted acoustic pressure to the outside of the pipe correspond to modal frequencies. To evaluate the transmission of the generated acoustic pressure, the effect of the structural-acoustic coupling should be taken into consideration.

REFERENCES

1. Wagner C, Hüttl T, Sagaut P. Large-Eddy Simulation for Acoustics. Cambridge University Press, 2007.
2. Curle N. The influence of solid boundaries on aerodynamic sound. Proc. Roy. Soc. (London). 1955; Vol. A 231. pp.505-514.
3. Ffowcs Williams J.E, Hawkings D.L. Sound generation by turbulence and surfaces in arbitrary motion. Philosophical Transactions of the Royal Society Series A. 1969; 264, pp.321-342.
4. Lighthill M. On sound generated aerodynamically, I. General theory. Proc. Roy. Soc. (London). 1952; Vol. A 211, pp.564-587.
5. Lighthill M. On sound generated aerodynamically, II. Turbulence as source of sound. Proc. Roy. Soc. (London). 1954; Vol. A 222, pp.1-32.
6. ANSYS CFX version 15.0 User's Guide. ANSYS Inc.
7. ANSYS Fluent version 15.0 User's Guide. ANSYS Inc.
8. WAON Users' Guide. Cybernet Systems CO., LTD.
9. ANSYS Mechanical version 15.0 User's Guide. ANSYS Inc.
10. Zdravkovich M.M, Flow around circular cylinders, Vol.1: Fundamentals. Oxford University Press, 1997.
11. Yokoyama H, Iida A. Aerodynamic sound from flows around a rectangular cylinder with a low mach number. Transactions of the JSME (in Japanese). 2013; Vol.79. No.799.
12. Ishihara K. Prediction of aerodynamic sound radiated from cylinder based on experimental data. Transactions of the JSME (in Japanese). 1999; Vol.65. No.638.
13. Ishihara K. Study on Acoustics and Flow Noise Characteristics of Bending Duct. Transactions of the JSME (in Japanese). 2011; Vol.77. No.776.